Terrestrial shallow water hydrothermal outflow characterized from out of space

Jean-Emmanuel Martelat, Javier Escartin, Thibaut Barreyre

▶ To cite this version:

Jean-Emmanuel Martelat, Javier Escartin, Thibaut Barreyre. Terrestrial shallow water hydrothermal outflow characterized from out of space. Marine Geology, 2020, 422, pp.106119. 10.1016/j.margeo.2020.106119 . insu-03251261

HAL Id: insu-03251261
https://insu.hal.science/insu-03251261

Submitted on 19 Oct 2021

Terrestrial shallow water hydrothermal outflow characterized from out of space

Jean-Emmanuel Martelat[a], Javier Escartín[b], and Thibaut Barreyre[c]

[a]Université de Lyon, UCBL, ENSL, CNRS, Laboratoire de Géologie LGL-TPE, 69622 Villeurbanne, France

[b]Université de Paris, Institut de Physique du Globe de Paris, CNRS, F-75005, France

[c]Department of Earth Science / K.G. Jebsen Centre for Deep Sea Research, University of Bergen, Bergen, Norway

Corresponding author. *E-mail address:* jean-emmanuel.martelat@univ-lyon1.fr

Laboratoire de Géologie de Lyon, Université Claude Bernard Lyon1, CNRS, 2, rue Raphaël Dubois Bât. GEODE 69622 Villeurbanne Cedex

Abstract

We investigate the potential of satellite imagery to map and monitor the activity of shallow-water hydrothermal systems, which are often found at volcanic islands. For this study, we used publicly available data and proprietary WorldView-2 satellites images, with spectral bands that can penetrate up to water depths of 30 m. Shallow water hydrothermal sites are visible on satellite imagery, primarily with publicly available data, demonstrating the potential of satellite imagery to study and monitor shallow water hydrothermal activity. We focus our work on volcanic islands, showing intense near-shore, shallow-water hydrothermal activity, and distinct styles of hydrothermal venting. Satellite imagery constrains regional outflow geometry and the temporal variability or stability of these systems. Milos Island shows hydrothermal outflow associated with reflective mineral precipitates and/or bacterial mats, which are stable over time (2010-2014). These outflows locally define polygonal patterns likely associated with hydrothermal convection in porous media. In Kueishantao Island individual hydrothermal plumes charged with particles are visible at the sea surface, and display great variability in intensity and distribution of plume sources (2002-2019). Worldwide we have identified ~15 shallow water hydrothermal sites with satellite imagery, that are similar to either the Milos system (e.g., Vulcano and Panarea, Italy), or the Kueishantao system (numerous sites in Pacific volcanic islands). This study demonstrates that satellite imagery can be used to map and monitor different types of shallow-water hydrothermal systems, at regional scale, and monitor their evolution. Satellite data provides not only regional and temporal information on these systems, unavailable to date, but also the regional context for follow-up *in situ* field data and observations (e.g., instrumental monitoring, sampling, observations and mapping with divers or AUVs) to understand both the nature and dynamics of these systems, and ultimately the associated fluxes.

Keywords: Shallow water; Seafloor mapping; Hydrothermal activity; Satellite imagery; Volcanic island.

1. Introduction

Submarine hydrothermal activity is common at volcanically active areas (e.g., mid-ocean ridges, seamounts, volcanic arcs), controlling heat and chemical exchanges through the seafloor. Mapping is critical to locate hydrothermal outflow, characterize its geometry, and document temporal variability. This mapping also provides context for instrumental measurements and sampling (e.g., temperature of outflow, chemistry, etc.). Numerous deep-sea vents are identified by local hydrothermal plumes detected in the water column (Baker et al., 1995; Baker and German, 2004; Baker et al., 2016), and subsequently surveyed acoustically and optically, and instrumented for monitoring (Barreyre et al., 2012, 2014a, 2014b; Barreyre and Sohn, 2016; Wilcock et al., 2016; Nooner and Chadwick, 2016; Baker et al., 2019). While numerous shallow-water (<200-300 m) hydrothermal systems have been identified (e.g., see Table 1 in Price and Giovannelli, 2017), we lack systematic and extensive optical surveys of these, hence their detailed extent, structure, and evolution are not documented. This information is also critical to understand the link to underlying heat sources, and the thermal, mass and chemical transfer between the solid Earth and the overlying ocean.

Satellites provide temporal series of high-resolution images throughout the Earth's surface acquired with various sensors. Specific spectral bands can penetrate shallow-water areas, and are used in coastal studies for benthos mapping (e.g. corals, seagrass), and estimation of near-shore bathymetry, (Eugenio et al., 2015; Reshitnyk et al., 2014; Baumstark et al., 2016; Dattola et al., 2018). To our knowledge, the only study of shallow water hydrothermal systems using satellite data monitored and documented a +1°C surface temperature anomaly over the 10-m deep Punta Mita site in Mexico (Torres-Vera et al, 2010), which is not visible in satellite imagery.

Satellite can document temporal variability of submarine hydrothermal activity, and ultimately evaluate the associated fluxes associated with these sites; optical surveys coupled to instrumental measurements, have been successfully applied to study deep-sea hydrothermal sites (Barreyre et al., 2012). Here we evaluate the use of satellite imagery to observe and monitor shallow-water hydrothermal activity, and at a low cost relative to repeated, extensive field surveys. Remotely-detected anomalies in hydrothermal activity may be ultimately linked to deep-seated processes (e.g., magmatic activity, seismicity), and contribute to hazard (e.g., phreatic explosions) and risk assessment near populated areas. Finally, the study of terrestrial hydrothermal systems using satellite data may provide insight into the potential indicators of hydrothermal activity at the surface of extraterrestrial bodies (e.g., Collins et al., 2000; Vance et al., 2007; Osinski et al., 2013).

In this pilot study we demonstrate that we can investigate shallow-water hydrothermal activity with satellite views, using both publicly available images, and WorldView-2 data provided by the Digital Globe Foundation. Image analyses reveal two different types of hydrothermal manifestations in satellite imagery (Figs. 1, 2). Firstly, satellite data directly image hydrothermal outflow zones at the seafloor, at depths of up to 30 m (Fig. 2a), owing to the high reflectivity of associated hydrothermal deposits, microbacterial mats, or both. We can thus map the hydrothermally active zones, and monitor potential temporal variations in their geometry. Secondly, we document turbidity at the sea surface due to hydrothermal plumes, which is the most common manifestation seen in the satellite imagery reviewed (Fig. 2b, Chen et al., 2018), and that documents the intensity of the hydrothermal activity and spatial distribution of plumes.

The Milos (Greece) shallow water hydrothermal system (Fig. 2a) shows seafloor patterns visible from space and is our main target. Prior studies of this site (e.g., Aliani et al., 1998; Aliani et al., 2004; Naden et al., 2005; Price et al., 2013) provide both ground-truthing and background information to validate satellite imagery interpretations, mapping, and characterization of this hydrothermal system. Available images from 2010, 2011 and 2014 also allow us to document temporal stability or variability. We also explore similar sites elsewhere (e.g., Panarea and Vulcano in Italy, Fig. 1, Table 1, and section 5.1.2).

We also evaluate the spatial monitoring of hydrothermal plumes reaching the sea surface at Kueishantao (Taiwan, Fig. 2b, Chen et al., 2018). Here satellite imagery documents variations in the intensity of the turbidity plumes, and their appearance and disappearance over time. Figure 1 and Table 1 locate and list all shallow-water hydrothermal systems with associated turbidity plumes visible on satellite images.

Finally, we evaluate the untapped potential of satellite imagery to better understand hydrothermal activity in shallow water environments, including its distribution, geometry, and temporal variability.

2. Datasets and methods

This study uses satellite imagery provided through Google-Earth, Ping Microsoft, EOS viewer, Wayback viewer by ESRI and Copernicus ESA (Table 1). These portals use images from various satellites (Sentinel, SPOT, Pleiades, Quickbird, WorldView-2 and 3) with resolutions ranging from 10 m to 1.24 m for multispectral images, that can be pansharpened with panchromatic images (2.5 to 0.31 m resolution, Ieronimidi et al., 2006). Archived imagery also provides sets of images acquired at different times at several sites. We report here the publicly available imagery used for the different shallow water hydrothermal sites studies in Table 1, together with the acquisition date. These images were selected by visual inspection, based on the absence of large waves, cloud-free scenes, and visibility of the hydrothermal activity offshore.

We complemented our study with WorldView-2 (WV2) satellite images provided by the Digital Globe Foundation (Table 2). The WV2 satellite collects both panchromatic and multispectral images of scenes of ~6.4 km x 18.0 km, with high spatial resolution of 0.46 m for imagery acquired at 450-800 nm, and 2 m for that acquired in 4 or 8 bands covering 396-1043 nm wavelengths. WV2 acquires images at spectral bands that penetrate water: coastal band 1 (396-458 nm), band 2 Blue (442-515 nm), and band 3 Green (506-586 nm), thus well-suited for littoral mapping at a regional scale down to water depths of up to ~30 meters (e.g., Eugenio et al., 2015; Koedsin et al., 2016; Collin et al., 2017).

The Digital Globe Foundation provided 13 WV2 images over our main study site, Milos (Greece). After rigorous visual inspection, we selected 4 suitable images for this study (Table 2). These clear-visibility scenes (wave- and cloud-free) reveal hydrothermal features with only smooth processing (interactive stretching in region of interest). The Digital Globe Foundation also provided 37 images from Panarea from which we selected 4 WV2 images (Italy, Table 2). WV2 satellite images were processed using ENVI standard procedures. We interactively stretched histograms in region of interest (Figs. 4a, 5b-d, 6a, 8a). In some other cases we also used multispectral analyses over the 8 available bands of the WV images, including principal component analyses (Figs. 3, 4b, 8c, d), and forward minimum noise fraction transform (Figs. 6b, c). Multispectral analyses gave highly contrasted black and white pictures, with smoothing sunlight reflection on waves. The different optical restitutions facilitated the mapping and interpretation (Fig. 4c).

We note that for data provided via a public source or through the Digital Globe Foundation, visual inspection of a large set of views was essential to obtain the best images of the seafloor hydrothermal systems. We also note that many images obtained during periods with no cloud cover or significant waves lack visible hydrothermal patterns.

3. Geological setting and prior work of studied submarine hydrothermal systems

3.1. Milos (Greece)

Milos Island, in the Hellenic Volcanic Arc, resulted from a Late Pliocene to late Pleistocene - Holocene volcanic pulse with submarine to subaerial eruptions emplaced on Mesozoic metamorphic basement and Neogene sediments (Fytikas et al., 1986; Stewart and McPhie, 2006). Intense offshore hydrothermal activity is correlated with tectonic activity (Papanikolaou et al., 1993; Dando et al., 1995b, Aliani et al., 2004; Nomikou et al., 2013; Yücel et al., 2013). Manifestations of this hydrothermal activity include gas emissions, high temperature fluids, microbacterial mats and precipitates of hydrothermal minerals (Fitykas and Marinelli 1976; Liakopoulos, 1987; Dando et al., 1995a; Valsami-Jones et al., 2005; Gilhooly et al., 2014). The Milos submarine hydrothermalism is best studied at the Paleochori Bay, to the SE of the island, through various methods, including echo sounding, divers, submarine robots (ROVs), and drones (Dando et al., 1995a, Price et al., 2013; Gilhooly et al., 2014; Godelitsas et al., 2015; Teague et al., 2018, Durán-Toro et al., 2019). Venting includes free-gas (CO_2, H_2, H_2S, CH_4) variably mixed with seawater, and fluids that are saline and sulphidic, depleted in Mg^{2+} and SO_4^{2-}, and enriched in As and metals (Fitzsimons et al., 1997; Valsami-Jones et al., 2005; Wu et al. 2011, 2016; Price et al., 2013; Gilhooly et al. 2014; Godelitsas et al., 2015). This hydrothermal activity results in yellow-orange and whitish precipitates respectively made of As-sulfide and a mix of sulfur and silica (Price et al., 2013; Yücel et al., 2013, Durán-Toro et al., 2019). The coupled hydrothermal, geochemical, and biogenic processes here are also intimately linked to microbial communities (e.g., Houghton et al., 2019). Locally, gas flow rates have been measured underwater (0.2 to 18.5 $l.h^{-1}$, Dando et al., 1995a) or at vent surfaces (<0.1 to 229 $ml.m^{-2}.min^{-1}$, Botz et al., 1996), but no site-wide estimates is available to date. Temporal monitoring of the hydrothermal outflow temperature has also been conducted, but at a limited number of sites and over ~ 3 months (Dando et al., 1995a; Aliani et al., 2004; Yücel et al., 2013), showing tidally driven variations.

Despite all these studies, we lack a comprehensive and coherent view of the hydrothermal activity at Paleochori Bay (and elsewhere along the Milos shoreline). Prior studies are often local (e.g., Gilhooly et al., 2014; Price et al., 2013), and observations are not properly replaced in a regional map showing the distribution, structure, and geometry of hydrothermal outflow. Figure 3 compiles available observations of hydrothermally active areas, and of point measurements of temperature of fluids and/or sediments in Paleochori Bay available in the literature. Processed WV2 satellite imagery in the background reveals the outflow in white and, to a first order, field measurements correlate with hydrothermal outflow features that we describe in detail below.

Table 1 reports additional sites along the Milos coast, where the seafloor images reveal similar patterns to those found at Paleochori (Spathi, Voudia, and Agia Kiraki Bays), in Panarea (Italy, see also Table 2), Vulcano (Italy) and Ko-Takara-Jima (Japan, Table 1).

3.2. Kueishantao (Taiwan)

Shallow-water hydrothermal activity along the southern coast of the Kueishantao Island displays prominent hydrothermal plumes reaching the sea surface and observable in satellite imagery (Chen et al., 2018). Kueishantao, located between the Okinawa Trough and the Philippines basin, hosts recent magmatic activity attributed to extension of the Okinawa Trough, with the most recent eruption dated around 7 ka (Chen et al., 2001). Hydrothermal venting is well-studied (e.g., Chen et al., 2005; Yang et al., 2012; Chen et al., 2016; Lin et al., 2019), and is associated with highly acidic fluids (pH ~2.5-3) venting at temperatures of up to ~120°C and with free gases, mainly CO_2 (Chen et al., 2005; Chen et al., 2016). These plumes are also particle-rich, discharging whitish and yellow fluids, depending on the concentration of sulfur particles (Chen et al., 2001; Han et al., 2014). Gas geochemistry indicate both magmatic degassing and interaction of fluids with marine sediments at depth (Chen et al., 2016), and likely indicate a magmatic system located beneath this island, as indicated by recent seismic studies (Lin et al., 2018). This area is seismically active, owing to both the underlying subduction and intra-arc extension (e.g., Lin et al., 2018), and a possible 2005 diking event associated with the Ilan earthquake (Lai et al., 2009). Seismic activity and extreme meteorological events have induced transient changes of this system, and in situ observations document a decline in the intensity of the hydrothermal activity, in addition to variations in the chemistry and degassing of the system (Lebrato et al., 2019). Overall, both in situ observations (Lebrato et al., 2019) and satellite imagery suggest a significant, recent decrease of hydrothermal activity here.

Table 1 reports several additional sites where similar hydrothermal plumes and associated turbid waters are visible from space. All the sites are located along the shore of volcanic areas, mainly in the Pacific. Sites include the active Nishinoshima volcano (Japan), which shows hydrothermal plumes associated with the recent lava flows.

4. Results

4.1. Seafloor hydrothermal seepage mapping at Paleochori Bay

Figure 4a shows a RGB composition from WV2 bands 1, 2, 3, showing white features at Paleochori and at Agia Kyriaki Bays. Figure 4b corresponds to the band 3 from a PCA processing on 8 bands, showing zones of varying grey tones throughout the two bays, which are visible to water depths of ~ 20 m. These patterns correspond to either seagrass meadows, or to hydrothermal features, as interpreted in Figure 4c, and described below.

First, light grey zones in Figure 4b dominate and constitute the background at the bays from the sea shore towards the off-shore, where the seafloor is no longer visible in the satellite imagery. These areas consist of sandy seafloor, and locally scattered seagrass *Cymodocea nodosa* (Aliani et al., 1998). Darker grey areas, found farther from the shore, display curved limits and consist of dense *Posidonia oceanica* seagrass meadows occluding the seafloor (Aliani et al., 1998). Visibility of *seagrass* meadows has facilitated numerous satellite studies of *Posidonia* (e.g., Godet et al., 2009; Costantino et al., 2010) or other species (e.g., Baumstark et al., 2016).

Second, the imagery also reveals complex patterns of white seafloor, defining lineations, connected polygons, isolated spots, and diffuse patches (Figs. 3, 4). These patterns are observable both in the processed WV2 images, and in the publicly available imagery (e.g., Google Earth, Wayback ESRI, see Table 1 and Fig. 2a) as highly reflective, white areas visible through the water column. We attributed this highly reflective association of hydrothermal activity with precipitates of white hydrothermal minerals, development of microbacterial mats, or both as is well documented in Paleochori Bay (e.g., Yücel et al., 2013; Price et al., 2013). The association of microbacterial mats and hydrothermal precipitates yields highly reflective areas that are readily recognizable optically. Such features are common in deep-sea hydrothermal systems, where photomosaics have been used to map their geometry and temporal evolution of fluid outflow at the seafloor, and of associated ecosystems (Barreyre et al., 2012; Marcon et al., 2014). Moreover abundant temperature measurements of fluids and gas in the area (Aliani et al., 1998, 2004, Botz et al., 1996, Dando et al., 1995a, Gilhooly et al., 2014, Durán-Toro et al., 2019), and aerial photography at Paleochori (see Figure 1 in Durán-Toro et al., 2019) correlate well with the white areas visible in the satellite imagery (Fig. 3). Hence, based both on satellite imagery and *in situ* observations (Aliani et al., 1998, 2004, Botz et al., 1996, Dando et al., 1995a, Gilhooly et al., 2014, Durán-Toro et al., 2019), the white seafloor features in Paleochori Bay, and at other bays along the coast of Milos, at Panarea, and at Vulcano, are clear indicators of active hydrothermal outflow.

The mapping in Paleochori Bay shows that no hydrothermal activity is observed in the immediate vicinity of seagrass meadows (Fig. 4). This confirms reports by Aliani et al. (1998), as neither *Posidonia oceanica* nor *Cymodocea nodosa* develop in areas where the subseafloor (~10 cm) shows temperatures >2.5°C above that of ambient seawater.

Finally, we observe seafloor with a darker tone than that of the seagrass meadows described above, and localized primarily within Agia Kiriaky Bay, West of Paleochori Bay (Fig. 4b). These darker seafloor zones consist of lineations that in some cases form polygons, which have diameters of 20 to 60 m (Fig. 4b SW region). We lack *in situ* observations that can be associated with these features. Based on their geometry and on their apparent association with the white, hydrothermally active areas, we speculate that these lineations may correspond to darker As-rich hydrothermal sulfides (Dando et al., 2000; Price et al., 2013), or to inactive, fossil outflow zones with altered and dark hydrothermal materials as described at deep-sea hydrothermal sites (Barreyre et al., 2012).

The mapping of the different areas shown in Figure 4c both at Paleochori and Agia Kyriaki, based on a WV2 image acquired in 2013, yields a total surface of ~60000 m^2 associated with white, hydrothermally active seafloor, corresponding to ~2% of the map surface, while the seagrass meadows cover ~19% of the seafloor in this area. Black areas, of possible hydrothermal origin, account for <1% of the seafloor.

4.2. Distribution of hydrothermal outflow at the scale of Milos Island

The detailed satellite-based mapping of the Paleochori Bay seafloor, supported by published *in-situ* observations, allow us to extrapolate our interpretation to other zones along the Milos shore (Fig. 5b). Patterns similar to those found in Paleochori and Agia Kyriaki Bays (Fig. 4) are clearly identifiable in the Voudia Bay (NE of Milos Island, Fig. 5c) and in Spathi, immediately East of Paleochori (Fig. 5d, Table 1). At these sites we identify structures similar to those at Paleochori Bay (lineations, connected polygons and patches). Observations at Voudia Bay are hindered by white water plumes derived from unconsolidated material emanating from exploited quarries of industrial minerals (bentonite and barite). We also observed similar bentonite-sourced white material about 1 km north of Spathi (Fig. 5b). These white sediments may be misinterpreted as white hydrothermal features, and may also cover hydrothermal outflow patterns in the area. The mapping of highly reflective, white seafloor both at Spathi and Voudia Bays indicates that ~1.7% of the seafloor is associated with active hydrothermal outflow, a proportion that is comparable to that found at Agia Kyriaki and Paleochori Bays (Fig. 4). Other reported hydrothermal sites in Milos Bay close to Adamas or close to the airport (Fig. 5a, Dando et al., 1995a; Valsami-Jones et al., 2005) are not visible in satellite imagery and *in situ* instead of satellite mapping would be required instead.

4.3. Tracking the evolution of hydrothermal activity in Milos

In addition to providing constraints on distribution and geometry of hydrothermal activity (Figs. 4, 5), satellite images acquired at different times document the stability and evolution of the hydrothermal outflow. From our set of satellite images over Paleochori Bay we select two WV2 multispectral images (August 18th 2011 and August 30th 2014), in addition to a panchromatic WV2 (November 16th 2010), all imaging the seafloor (Fig. 6) and thus constraining the evolution of hydrothermal outflow geometry over 4 years.

The comparison of images acquired at different times (Fig. 6) indicates that the geometry of the hydrothermal system is stable over a few years, and that the visible changes are minor and local, and do not modify the overall structure. For example, the larger hydrothermal patch at the center of Fig. 6 displays significant reflectivity variations within but shows stable boundaries over this period of time. While we do not have imagery to evaluate variations at shorter temporal scales (e.g., seasonal changes, storms, over a few weeks to a few days), Yücel et al. (2013) observed the rapid development of microbacterial mats following a period of significant wind-driven wave action, with seafloor patterns re-established in less than 3 days. This reported observation, together with the imagery available (Fig. 6, Tables 1 and 2), suggests a multi-year stability of the system and an overall geometry unaffected by short-term meteorological events (e.g., winter storms, strong winds and associated waves).

4.4. Temporal variability from hydrothermal plume observations

The Kueishantao hydrothermal field (Fig. 7) shows a complex temporal evolution, with variations in the number, location, and intensity of hydrothermal plumes imaged at the sea surface. In addition to temporal variations in hydrothermal activity, these satellite images also reveal the strong influence of currents sweeping the area on plume dispersion. These plumes are associated with near-shore vents mapped at water depths of up to ~30 m (e.g., Chen et al., 2005; Yang et al., 2012). The vents discharge high-temperature fluids rich with CO_2 (e.g., Lin et al, 2019). These observations of the sea surface do not constrain the hydrothermal activity at the seafloor, as is the case for the Milos systems, and therefore inferences on variations and distribution of hydrothermal activity are qualitative and indirect.

Despite these limitations, satellite views document a decrease in the site's hydrothermal activity from the early 2000's to 2016 (Fig. 7), which is consistent with reported in-situ observations (e.g., Chen et al., 2018; Lebrato et al., 2019). Owing to the currents, it is difficult to determine if observed variations at short time-scales (a few weeks to months) correspond to actual variations in overall hydrothermal fluxes, or, alternatively, to water column processes (currents, waves), which control plume dispersion. This system shows transient behavior as a result of seismicity and major weather events (Lebrato et al., 2019).

Satellite images also suggest that hydrothermal outflow geometry at Kueishantao varies significantly over time, consistent with overall flux variations. Plume sources appear and disappear over time, and the temporal persistence of individual plumes is highly variable (Fig. 7). Lacking imagery that is regularly spaced in time, we cannot accurately constrain the life-span of individual vents. However, some vent sources are observed in a single image, suggesting that they are activated and deactivated over periods of time that vary between a few months and a year. These observations suggest that the Kueishantao system is more dynamic and variable than that of Milos, where persistent seafloor patterns indicate a stable outflow geometry over several years.

5. Discussion

5.1. Shallow water hydrothermal outflow: modes, temporal variability, and fluxes

5.1.1. Polygonal hydrothermal circulation

The well-defined, polygonal patterns of highly reflective hydrothermal deposits or bacterial mats identified at different bays along the southern and eastern coast of Milos (Figs. 4-6) are similar to seafloor features at the Baia di Levante on the Vulcano hydrothermal site (Fig. 8e). These white polygons vary in size from 1 m to up to ~25 m, and appear to develop in bays with a sandy bottom. While we lack *in situ* long-term instrumental data (e.g., temperature) to accurately monitor temporal variability, the satellite images suggest that the organization of hydrothermal deposits and microbacterial mats is associated with a stable sub-seafloor fluid flow geometry over periods of a few years. These hydrothermal polygonal structures are reminiscent of patterns that develop from free convection in porous media heated from below (e.g., Shattuck et al., 1997; Hennenberg et al., 1997; Tasaka et al., 2005; Nield and Bejan, 2006), described in the literature as the Horton-Rogers-Lapwood Problem (Horton and Rogers, 1945; Lapwood, 1948), a porous-medium analog of the Rayleigh-Bénard problem.

In situ studies in Milos also indicate that areas with white microbacterial mats are associated with higher fluid outflow temperatures than surrounding zones (Wenzhofer et al., 2000, Houghton et al., 2019). While we do not have a precise location of these measurements relative to the structures imaged with satellite, these results would suggest that seafloor patterns indicate hydrothermal upflow (i.e., higher temperature) at white seafloor areas (i.e., edges of polygons). The predicted sense of fluid motion in a hexagonal cell is driven by property variations of convecting fluids. Detailed studies of both the geometry and the temperature associated with these patterns (spatially and in depth), are required to constrain the associated hydrodynamic and thermal conditions (e.g., Nield and Bejan, 2006), and ultimately evaluate thermal and chemical fluxes when coupled with temperature and geochemical data. Satellite images also indicate that this polygonal organization of hydrothermal circulation is restricted in space, laterally transitioning to other modes of hydrothermal outflow (e.g., patches of diffuse flow, see below), that may indicate different hydrothermal circulation regimes.

5.1.2. Diffuse flow

In addition to polygonal patterns, we observe patches of white seafloor with irregular edges, often displaying variations in their surface (density of their color from white to grey, continuity). These patches, which we attribute to hydrothermal deposits and/or microbacterial mats as in the case of polygonal structures, are found at Paleochori and Spathi Bays (Figs. 5, 6) and Panarea (Fig. 8a), and maintain their overall geometry and extent over several years (Paleochori, Fig. 6 and Panarea, Figs. 8b,c,d). Visually similar patches are observed in deep-sea hydrothermal systems showing diffuse flow (Barreyre et al., 2012; Campbell et al., 2013), with intensity variations attributed to changes in the local hydrothermal flux (e.g., Barreyre et al., 2012). This observation thus suggests that in Paleochori and Voudia Bays both hydrothermal circulation organized in polygonal circulation and pervasive diffuse outflow at white seafloor patches co-exist and persist over several years.

5.1.3. Hydrothermal plumes

The polygonal and the diffuse hydrothermal circulation systems discussed above are likely associated with low flow rates with clear fluids relative to sites with focused venting, such as the Kueishantao particle-laden plumes (Fig. 7). Plumes imply elevated fluid outflow velocities at a point source, generating a jet and an associated turbulent plume that spreads in the water column (e.g., Speer and Rona, 1989). If water depth is sufficiently shallow or buoyancy flux sufficiently high, plumes can be observed at the sea surface (Fig. 7). While the satellite data acquired at

Kueishantao reveal plumes of different sizes, their geometry cannot be used to estimate fluxes as we lack *in situ* measurements on water depth, outflow temperature, or fluid exit velocity.

While plumes are observed at other shallow water hydrothermal systems at volcanic islands (Table 1), their nature differ from the Kueishantao plumes (Figures 7c-h). For example, the hydrothermal system in Nagahama Bay, Japan (Table 1) shows several discharge zones along the shoreline (Kiyokawa et al., 2012), with plumes derived from broad zones of outflow rather than a clear point source. The temporal study of this system (Kiyokawa et al., 2012) suggests a hydrothermal discharge coupled with the meteoric groundwater fluctuations along the coast. These systems thus show a coupling of hydrothermal activity with subaerial and subsurface processes (e.g., pluviometry) near shore, and differ with those at Kueishantao (Chen et al., 2005; Chen et al., 2018) and other deep sea vents (e.g., Barreyre et al., 2012; Mittelstaedt et al., 2012), where the focused flow and vents are controlled solely by deep-seated hydrothermal processes.

5.1.4. Temporal variability

Satellite imagery reveals that shallow water hydrothermal systems display both stability (e.g., Paleochori at Milos) and variability (e.g., Kueishantao, Chen et al., 2018) at time-scales of months to years. The patterns and distribution of hydrothermal deposits and microbacterial mats in areas with repeated imagery available (Milos, Panarea, Figs. 6, 8b-d), suggest that these systems, dominated by distributed flow and low flux rates relative to focused venting, are stable in the long-term (years to decades). In contrast, sites with focused and vigorous venting, such as Kueishantao

(Fig. 7, Chen et al., 2018), are highly dynamic systems, with possible unstable heat sources and/or fluid paths that lead to activation and deactivation of vents, in addition to variations in overall flux. Hence, in shallow-water systems with diffuse flow, variations in their distribution and geometry can be monitored from space.

Our satellite database cannot document very short-term variability (less than a few months) at shallow water hydrothermal systems (i.e., Milos, Kueishantao). Temperature records of hydrothermal outflow often show a tidal modulation, as shown for Milos (e.g., Aliani et al., 2006; Yücel et al., 2013), Kueishantao (Chen et al., 2005) or Panarea (e.g., Schipeck et al., 2011), and at deep-sea vents (e.g., Barreyre et al., 2014a, b). In addition to periodic variability, these systems may also show events over time as a response to deep-seated processes (e.g., seismicity, magmatic events, etc.) that may modify subseafloor permeability, heat sources location, or fluid paths. Stochastic events are common in deep-sea vents (e.g., Sohn 2007; Barreyre et al., 2014a), and documented at Panarea, with a gas outburst in 2002 associated with a change in the hydrothermal circulation at depth (e.g., Esposito et al., 2006; Tassi et al., 2014) that generated plumes visible on the sea surface (e.g., see Fig. 1 in Capaccioni et al., 2005). While this event was not captured in the satellite imagery that we have reviewed (Table 1), it would be visible in satellite imagery and therefore could be monitored from space in real time. Similarly, Milos has experienced similar events, attributed to seawater influx in the hydrothermal circulation system leading to sudden modifications of fluid temperature and chemistry of the hydrothermal fluids, possibly linked to microseismic activity (Aliani et al., 2004, Yücel et al., 2013). These events triggered temporal disappearance of microbacterial mats at the seafloor, with a subsequent recovery (Yücel et al.,

2013) (Fig. 6). As such events can be imaged from space, satellite imagery with high revisit frequency has the potential to identify and monitor variations in hydrothermal circulation and associated fluxes at different time-scales (from year to few days).

5.1.5. Fluxes

While numerous *in situ* studies have been conducted at some of our studied sites (e.g., Yücel et al., 2013; Valsami-Jones et al, 2005; Caracussi et al, 2005; Price et al., 2013; Tassi et al., 2014; Chen et al., 2016; see also Fig. 3), neither the fluid or chemical fluxes are constrained. Flux estimates require the systematic optical mapping of zones of fluid emissions and other hydrothermal features, to precisely locate instrumental measurements and samples, and to subsequently extrapolate these local observations to estimate fluxes (chemical, heat, and mass). For example, at the hydrothermal systems described in Milos (Agia Kyriaky, Paleochori, Spathi and Voudia Bays, Figs. 4, 5, Table 1), hydrothermally active areas corresponding to white patches and polygonal patterns represent between 1.7% and ~2% of the total mapped surface (~3.4 km^2). Calculation of fluxes would require integration of *in* situ temperature and fluid chemistry data from the mapped hydrothermal structures, an approach successfully applied at deep-sea hydrothermal systems (e.g., Barreyre et al., 2012; Escartin et al., 2015). Furthermore, *in situ* measurements and observations would also document hydrothermal activity that may not be associated with visible hydrothermal structures, and thus not considered in flux estimates based on optical mapping alone. Hence, satellite imagery has the potential to provide the geological context, the distribution and geometry of diffuse shallow water hydrothermal outflow (Figs. 3,5), in order to plan field work, and to ultimately allow flux estimation that is not feasible with *in situ* measurements alone.

5.2. Mappability of terrestrial submarine hydrothermal systems from space

5.2.1. Limitations

While this study demonstrates the possibility of mapping different types of shallow water hydrothermal systems using satellite imagery, several limitations are imposed by the imaging conditions, and by the nature of the hydrothermal systems. Numerous factors can preclude the observation of the seafloor, including water turbidity (e.g., sediment plumes), sun illumination angle, sea surface state, currents, winds, clouds, etc. Indeed, numerous satellite images in Milos or Panarea are unusable, resulting in inhomogeneous time series from one site to another, or at different time windows.

Hydrothermal plume sources can be identified in satellite imagery in certain sites (e.g., Kueishantao), but currents control their appearance, dispersion, and shape at the sea surface of hydrothermal plumes. Furthermore, the interaction between the hydrothermal system and groundwater circulation nearshore can also modify the hydrothermal plumes (e.g., Nagahama Bay, Kiyokawa et al., 2012). Hence, in these systems, the shape and size of plumes cannot be directly interpreted as an indicator of intensity of hydrothermal activity or as a proxy for associated fluxes, and additional parameters (e.g, meteorological data, pluviometry, hydrographic, sea state, and current data, etc.) are required to identify and evaluate the role of processes other than hydrothermal activity.

The nature of the submarine hydrothermal system controls its visibility from space. After careful review of satellite imagery, we have identified 15 hydrothermal systems (Table 1) from the >40 sites at water depths of up to 20-30 m identified in the literature (see compilation by Price and Giovannelli, 2017, and references therein). Sites not identified here may not exhibit visible hydrothermal features, such as hydrothermal precipitates, microbacterial mats, or hydrothermally-induced turbidity. For example free gas escapes through both sand and rocky seafloor (e.g., Champagne Springs, Caribbean) display no distinct texture nor color (e.g., Fig. 2 in Kleint et al., 2017), precluding their identification.

5.2.2. Regional mapping of shallow water hydrothermal systems

Satellite imagery provides a regional view of hydrothermal systems that is not captured with traditional *in situ* field survey methods. For example, hydrothermal activity has been reported at all the Milos sites shown in this paper but *in* situ observations cannot constrain properly the geometry and distribution of hydrothermal features over very large areas (e.g., Spathi and Voudia Bays, Fig. 5). We propose several approaches to further improve hydrothermal outflow characterization (i.e., nature and extent of the activity). First, a more complete library of satellite data available by different providers (with highest resolution, and adequate spectral measure from one satellite or aggregated images from different satellite taken at same time, Nikolakopoulos, et al., 2007, 2008) would increase the number of images at shallow water hydrothermal sites with more homogeneous data, adequate imaging conditions, and large time covering. Second, *in situ* field work (e.g., scuba-divers, robotic vehicles) at different spatial scales would provide a complete view of the hydrothermal system, and data co-registered with imagery to conduct well-constrained quantitative studies at regional scales (e.g. real extent of the outflow system and characterization of fluxes). Finally, the hydrothermal structures mapped from 0 to up to 30 meter depths may extend to deeper areas (e.g., up to 500 m in Milos, Dando et al., 1995), and studies with remotely operated vehicles or autonomous vehicles are required for the full characterization of these systems from the shore to the deep sea.

6. Conclusions

Satellite imagery is suitable to study shallow-water active hydrothermal systems, and in particular for (i) imaging hydrothermal outflow at the seafloor to depths of up to 30 m owing to reflective seafloor (hydrothermal deposits, microbacterial mats), and (ii) detecting turbidity at the sea surface associated with hydrothermal plumes. We have identified 15 shallow water hydrothermal systems worldwide in satellite imagery, and focus our study on Milos (Greece) and Kueishantao (Taiwan), two well studied and characterized sites, and with available satellite imagery spanning several years.

At Milos, satellite imagery reveals areas of well-organized, polygonal hydrothermal patterns with cells up to 25 m in width, and that are stable over several. The seafloor with reflective zones (active high-temperature outflow) covers ~2% of the studied surface at Milos. At Kueishantao the imaged hydrothermal plumes records a fluctuating activity over several years, with individual plumes varying in intensity, appearing and disappearing. Satellite data thus provide information on the extent and distribution of hydrothermal activity and its temporal evolution. These data are also critical to extrapolate *in situ* field observations and measurements (e.g., mapping with underwater vehicles, physical and chemical measurements), to estimate fluxes (mass, heat, chemical) associated with this fluid hydrothermal circulation, and focus new *in situ* field work, sampling, and instrumental monitoring.

Acknowledgements

The authors acknowledge the support from the Digital Globe Foundation, which provided WorldView satellite imagery used in this study. This study was partly funded by two SYSTER grants from CNRS/INSU to J.-E. M (2018), and to J. E. (2017). J.-E. M was also supported by the Université de Lyon (France), J.E. by CNRS and IPGP, and T. B. was supported by the University of Bergen and the K.G. Jebsen Centre for Deepsea Research (Norway). We thank the editor and the two anonymous reviewers for their helpful, thorough and constructive comments that helped us to significantly improve this paper.

Figure captions

Fig. 1. Active submarine hydrothermal sites visible on satellite images, either as seafloor structures linked to hydrothermal outflow (green dots) or hydrothermal plumes visible at the sea surface (red). See Table 1 for additional details on these sites. A synthesis of identified sites in the literature is available in review papers (e.g., Tarasov et al., 2005; Price and Giovanelli, 2017), and references therein.

Fig. 2: Satellite images showing hydrothermal activity identified as seafloor structures (Milos, Greece, UTM35-WGS84 coordinate system were used), a) or sea-surface turbidity from hydrothermal plumes (Kueishantao, Taiwan, b). Imagery is from Digital Globe, and obtained from (a) Google Earth viewer (2015/03/15), (b) Bing Microsoft images viewer (undated).

Fig. 3. Compilation of observations on the occurrence of hydrothermal activity and temperature measurements at Paleochori Bay. Temperatures were measured at different depths subseafloor and within the sediment. Red dots correspond to measurements reported by Aliani et al. (2004), and include a site monitored for 70 days (red dot with thick outline). The orange circle corresponds to the site studied by Botz et al. (1996), and the pink circles to vent sites and temperatures reported by Dando et al. (1995a). Green dots correspond to temperature measurements nearshore by Gilhooly et al. (2014) (SE: Spiegelei). The blue square shows the aerial imagery from Durán-Toro et al. (2019), and the blue line within the transect studied by these authors. RP: Rocky Point. Violet

and orange transparent areas correspond to seepage areas of highly saline and sulphidic brines (Fitzimons et al., 1997; Aliani et al., 1998). Background corresponds to multispectral WV2 image from 8 July 2013 (enhanced band 2, from Principal Component Analysis processing on 8 bands). Isobaths from Aliani et al. (1998). UTM35-WGS84 coordinate system were used.

Fig. 4. Mapping of the geometry and distribution of identified seafloor areas, including zones of interpreted hydrothermal outflow identifiable in satellite imagery at Milos, from Agia Kyriaki beach to Paleochori Bay. Multispectral satellite data (a) is processed to obtain images that enhance features visible at the seafloor (b), that are then used for detailed mapping (c). Seafloor is imaged adequately to depths of ~20 m. As in Figure 3, the 20-m isobaths in 4b are from Aliani et al. (1998). See text for discussion of the different seafloor features and zones interpreted in c). Multispectral WV2 image from 8 July 2013: (a) RGB composition bands 1, 2, 3 (b) enhanced band 3, from PCA processing on 8 bands. UTM35-WGS84 coordinate system were used.

Fig. 5. Milos Island (a) and overview of seafloor hydrothermal features identified from satellite imagery along the SE coast (b) and detailed view of Spathi and Voudia Bays (c,d). White and reflective seafloor showing textures similar to those presented in figure 4, and defining polygonal patterns, lineations, and patches, are found at different sites of Milos. We also indicate white sediment from a landslide (black arrow). Multispectral WV2 image acquired 8 July 2013 with RGB composition on bands 1, 2, 3 respectively. On figures (c) and (d) the white, reflective seafloor represents ~1.7% of the mapped seafloor surface. UTM35-WGS84 coordinate system were used.

Fig. 6. Set of images from Paleochori Bay (Figs. 4b) showing the overall temporal stability of the hydrothermal outflow geometry between 2010 and 2014. Red ellipses indicate the same areas to facilitate comparisons among images. Images where acquired in (a) 16 November 2010 panchromatic, (b) 18 August 2011 multispectral, (c) 30 August 2014 multispectral. The image were acquired under different conditions: image (a) has different resolution and was acquired at different spectral wavelength, image (b) was acquired under windier and wavier conditions than those of the other two images. The panchromatic images were stretched. For multispectral images stretching was done on images obtained by forward minimum noise fraction transform on 8 available bands: resulting band 3 and band 4 for (b) and (c) respectively.

Fig. 7. Kueishantao Island north-east Taiwan showing the temporal variations in hydrothermal plumes evolution visible at the sea surface and spanning 17 years. White arrows indicate active sites, red arrows new sites, grey transparent arrows inactive sites relative to prior image. The yellow arrow localized breaking waves on a rock peak. Google-Earth viewer images from Digital Globe satellite (a, b, c, e) and CNES/Airbus image source (satellite not indicated), (g), ESRI Wayback Imagery from WV2 satellite (d), and Sentinel-2 imagery (Copernicus viewer, h).

Fig. 8. Distribution and temporal evolution of hydrothermal structures near Bottaro Island (Italy), hosting the Panarea hydrothermal site (a-d), and of Vulcano (Italy) (e). At Bottaro Island (a-d), hydrothermal activity is associated with light grey to white areas corresponding to white

biofilms, sulfur precipitates, brine concentration and the absence of Posidonia plants. Red dots indicate main exhalative centers with bubbles obtained by multibeam echo sounding surveys performed between December 2002 and December 2003 (published maps from Anzidei et al., 2005; Esposito et al., 2006). White sand sourcing from the island is trapped in depressions. The rest of the seafloor, partly covered by *Posidonia* mats, consists of loosely to consolidated Holocene sands, gravels and conglomerates derived from lava erosion (Esposito et al., 2006). (a) WV2 multispectral image 25 July 2014. (b,c,d) monochromatic WV2 images from three dates of view, the small square shows stability of a white patch : (b) 9 October 2010, stretched panchromatic image; (c) 3 August 2013, stretched band 4 from PCA analyses on 8 bands; (d) 25 July 2014, band 3 from PCA analyses on 8 bands. (e) Baia di Levante at Vulcano Island where two vents has been studied (Capasso et al., 1997, Amend et al., 1998, Skoog et al., 2007). This area shows a polygonal pattern (few meters to 10 meters in diameter) that likely corresponds to structures that are similar to those from Milos. Google-Earth images, July-2017. UTM33-WGS84 coordinate system were used.

Tables

Table 1

Shallow water hydrothermal systems visible from Space, and corresponding publicly available imagery. A synthesis of identified sites in the literature is available in review papers (e.g., Tarasov et al., 2005; Price and Giovanelli, 2017), and references therein.

(1) Imagery names identify access through Google Earth (GE) or Wayback ESRI's viewer (WB). Numbers indicate the year, month and date of scene acquisition (YYYMMDD). World View satellites are the main source of imagery for both GE and WB viewers, although imagery without the satellite source is also provided (e.g. CNES/Airbus source that may correspond to SPOT images).

(2) In the case of the Kueishantao, Methana, and Nea and Palea-Kameni hydrothermal fields, we provide a qualitative indication of the degree of hydrothermal activity, classified as high, medium, low, and no activity (HA, MA, LA, NA), respectively, and based on the number and intensity of recognizable turbid hydrothermal plumes at the sea surface.

(3) In Methana hydrothermal activity near-shore is also visible on a near-shore artificial lagoon. Plumes observed in the satellite imagery may correspond to seepage from this lagoon, in addition to or instead of local seepage at the seafloor nearby.

Table 2

World-View remote sensing data (LV2A, WV2 images) for Milos (Greece) and Panarea Islands (Italy), provided by the Digital Globe Foundation.

References

Aliani S., Bianchi N., Cocito S., Dando P. R., Meloni R., Morri C., Adelbert A., Peirano A., Ziebis W., 1998. A map of seagrass meadows in Palaeochori Bay (Milos Island, Greece), a marine aera with hydrothermal activity. Rapports et Procès Verbaux-Commission Internationale pour l'Exploration Scientifique de la mer 35, 512-513.

Aliani, S., Meloni, R., Dando, P. R., 2004. Periodicities in sediment temperature time-series at a marine shallow water hydrothermal vent in Milos Island (Aegean Volcanic arc, Eastern Mediterranean). J. Marine Syst. 46, 109-119.

Amend, J. A. N. P., Amend, A. C., Valenza, M., Palermo, Á., Applicazioni, T., 1998. Determination of volatile fatty acids in the hot springs of Vulcano, Aeolian Islands, Italy. Org. Geochem. 28, 699-705.

Anzidei, M., Esposito, A., Bortoluzzi, G., De Giosa, F., 2005. Thae high resolution bathymetric map of the exhalative area of Panarea (Aeolian Islands, Italy). Ann. Geophys-Italy 48, 899-921.

Baker, E. T., German, C. R., Elderfield, H., 1995. Hydrothermal plumes over spreading-center axes: global distributions and geological inferences. Geophys. Monog. AGU 91, 47-47.

Baker, E. T., German, C. R., 2004. On the global distribution of hydrothermal vent fields. Mid-Ocean Ridges: Hydrothermal Interactions Between the Lithosphere and Oceans. Geophys. Monogr. Ser. 148, 245-266.

Baker, E. T., Resing, J. A., Haymon, R. M., Tunnicliffe, V., Lavelle, J. W., Martinez, F., Ferrini V., Walker S.L., Nakamura, K., 2016. How many vent fields? New estimates of vent field populations on ocean ridges from precise mapping of hydrothermal discharge locations. Earth Planet. Sci. Lett. 449, 186-196.

Baker, E. T., Walker, S. L., Chadwick Jr, W. W., Butterfield, D. A., Buck, N. J., Resing, J. A., 2019. Posteruption Enhancement of Hydrothermal Activity: A 33- Year, Multieruption Time Series at Axial Seamount (Juan de Fuca Ridge). Geochem. Geophys. Geosyst. 20, 814-828.

Barreyre, T., Escartín, J., Garcia, R., Cannat, M., Mittelstaedt, E., Prados, R., 2012. Structure, temporal evolution, and heat flux estimates from the Lucky Strike deep- sea hydrothermal field derived from seafloor image mosaics. Geochem. Geophys. Geosyst. 13, 4, Q04008. https://doi:10.1029/2011GC003990.

Barreyre, T., Escartín, J., Sohn, R. A., Cannat, M., Ballu, V., Crawford, W. C., 2014a. Temporal variability and tidal modulation of hydrothermal exit- fluid temperatures at the Lucky Strike deep- sea vent field, Mid- Atlantic Ridge. J. Geophys. Res. Solid Earth, 119, 2543-2566.

Barreyre, T., Escartín, J., Sohn, R., Cannat, M., 2014b. Permeability of the Lucky Strike deep-sea hydrothermal system: Constraints from the poroelastic response to ocean tidal loading. Earth Planet. Sci. Lett. 408, 146-154.

Barreyre, T., Sohn, R. A., 2016. Poroelastic response of mid-ocean ridge hydrothermal systems to ocean tidal loading: Implications for shallow permeability structure. Geophys. Res. Lett. 43, 1660-1668.

Baumstark, R., Duffey, R., and Pu, R., 2016. Mapping seagrass and colonized hard bottom in Springs Coast, Florida using WorldView-2 satellite imagery. Estuarine Coastal Mar. Sci. 181, 83–92. https://doi: 10.1016/j.ecss.2016.08.019.

Bortoluzzi, G., Aliani, S., Ligi, M., D'Oriano F., Ferrante, V., Riminucci, F., Carmisciano C., Cocchi, L., Muccini, F., 2011. Multidisciplinary Investigations at Panarea (Aeo- lian Islands) after the Exhalative Crisis of 2002. Vol. Mare DTA/06-2011, Roma, pp. 1471-1488.

Botz, R., Stüben, D., Gisela, W., Bayer, R., Schmitt, M., Eckhard, F., 1996. Hydrothermal gases offshore Milos Island. Greece. Chem. Geol. 130, 161-173.

Campbell, B., Polson, S., Zeigler Allen, L., Williamson, S., Lee, C., Wommack, K., and Cary, S., 2013. Diffuse flow environments within basalt- and sediment-based hydrothermal vent ecosystems harbor specialized microbial communities. Front. Microbiol. 4, pp. 182.

Capaccioni, B., Tassi, F., Vaselli, O., Tedesco, D., Rossi, P. L., 2005. The November 2002 degassing event at Panarea Island (Italy): Five months of geochemical monitoring. Ann. Geophys-Italy 48, 755–765.

Capasso, G., Favara, R., Inguaggiato, S., 1997. Chemical features and isotopic composition of gaseous manifestations on Vulcano Island, Aeolian Islands, Italy: an interpretative model of fluid circulation. Geochim. Cosmochim. Acta 61, 3425-3440.

Caracausi, A., Ditta, M., Italiano, F., Longo, M., Nuccio, P.M., Paonita, A., Rizzo, A., 2005. Changes in fluid geochemistry and physico-chemical conditions of geothermal systems caused by magmatic input: The recent abrupt outgassing off the island of Panarea (Aeolian Islands, Italy). Geochim. Cosmochim. Acta 69, 3045–3059. https://doi: 10.1016/j.gca.2005.02.011.

Chen, Y. G., Wu, W. S., Chen, C. H., Liu, T. K., 2001. A date for volcanic eruption inferred from a siltstone xenolith. Quat. Sci. Rev. 20, 869–873. https://doi.org/10.1016/S0277-3791(00)00047-0.

Chen, C. T. A., Zeng, Z., Kuo, F. W., Yang, T. F., Wang, B. J., Tu, Y. Y., 2005. Tide-influenced acidic hydrothermal system offshore NE Taiwan. Chem. Geol. 224, 69-81. https://doi.org/10.1016/j.chemgeo.2005.07.022.

Chen, X.-G., Zhang, H.-Y., Chen, C.-T., Chen A., Yang, T. F., Ye, Y., 2016. The chemical and isotopic compositions of gas discharge from shallow-water hydrothermal vents at Kueishantao, offshore northeast Taiwan. Geochem. J. 50, https://doi:10.2343/geochemj.2.0425.

Chen, X.G., Lyu, S.S., Zhang, P.P., Yu, M.Z., Chen, C.T.A., Chen, Y.J., Li, X., Jin, A., Zhang, H.Y., Duan, W., and Ye, Y., 2018. Gas discharges from the Kueishantao hydrothermal vents, offshore northeast Taiwan: Implications for drastic variations of magmatic/hydrothermal activities. J. Volcanol. Geotherm. Res. 353, 1–10. https://doi: 10.1016/j.jvolgeores.2018.01.013.

Collin, A., Etienne, S., Feunteun E., 2017. VHR coastal bathymetry using WorldView-3: colour versus learner. Remote Sens. Lett. 8, 1072-1081. https://doi: 10.1080/2150704X.2017.1354261

Collins, G. C., Iii, J. W. H., Pappalardo, R. T., Spaun, N. A., 2000. Evaluation of models for the formation of chaotic terrain on Europa. J. Geophys. Res. 105, 1709-1716.

Costantino, G., Mastrototaro, F., Tursi, A., Torchia, G., Pititto, F., Salerno, G., Lembo, G., Sion, L., D'Onghia, G., Carlucci, R., Maiorano, P., 2010. Distribution and bio-ecological features of Posidonia oceanica meadows along the coasts of the southern Adriatic and Northern Ionian Seas. Chem. Ecol. 26, S1, 91–104.

Dando, P. R., Hughes, J. A., Leahy, Y., Niven, S. J., Taylor, L. J., Smith, C., 1995a. Gas venting rates from submarine hydrothermal areas around the island of Milos, Hellenic Volcanic Arc. Cont. Shelf Res. 15, 913-929.

Dando, P. R., Hughes, J. A., Leahy, Y., Taylor, L. J., Zivanovic, S., 1995b. Earthquakes increase hydrothermal venting and nutrient inputs into the Aegean. Cont. Shelf Res. 15, 655-662. https://doi.org/10.1016/0278-4343(94)E0031-G.

Dando P. R., Aliani S., Arabj H., Bianchi C. N., Brehmeg M., Cocito S., Fowle S. W., Guodersen J., Hooper L. E., Kiilbl R., Kuever J., Linke P., Makropoulos K. C., Meloni R, Mique J.-C., Morri C., Miiller S., Robinson C., Scblesne H., Sievert S., Stijhr R., Stiiben D., Thomm M., Varnavas S. P., Ziebis W., 2000. Hydrothermal studies in the Aegean Sea. Phys. Chem. Earth. 25, 1-8.

Dattola, L., Aramini, G., Scalise, S., Dominici, R., Di Mento, R., Lanera, P., Cappa, P., 2018. Comparison of Sentinel-2 and Landsat-8 OLI satellite images vs. high spatial resolution images (MIVIS and WorldView-2) for mapping Posidonia oceanica meadows. SPIEDigitalLibrary. 1078419, 42. https://doi.org/10.1117/12.2326798.

Durán-Toro, V. M., Price, R. E., Maas, M., Brombach, C. C., Pichler, T., Rezwan, K., Bühring, S. I., 2019. Amorphous arsenic sulfide nanoparticles in a shallow water hydrothermal system. Mar. Chem. 211, 25–36. https://doi.org/10.1016/j.marchem.2019.03.008.

Escartin, J., Barreyre, T., Cannat, M., Garcia, R., Gracias, N., Deschamps, A., Salocchi, A., Sarradin, P.M. Ballu, V., 2015. Hydrothermal activity along the slow-spreading Lucky Strike ridge segment (Mid-Atlantic Ridge): Distribution, heatflux, and geological controls. Earth Planet. Sci. Lett. 431, 173-185.

Esposito, A., Giordano, G., Anzidei, M., 2006. The 2002-2003 submarine gas eruption at Panarea volcano (Aeolian Islands, Italy): Volcanology of the seafloor and implications for the hazard scenario. Mar. Geol. 227.119-134.

Eugenio, F., Marcello, J., Martin, J., 2015. High-Resolution Maps of Bathymetry and Benthic Habitats in Shallow-Water Environments Using Multispectral Remote Sensing Imagery. Geoscience and Remote Sensing. IEEE Trans. Geosci. Remote Sens. 53, 3539-3549. https://doi.org/10.1109/TGRS.2014.2377300.

Fitzsimons, M. F., Dando, P. R., Hughes, J. A., Thiermann, F., Akoumianaki, I., Pratt, S. M., 1997. Submarine hydrothermal brine seeps off Milos, Greece : Observations and geochemistry. Mar. Chem. 57, 325-340.

Fytikas, M., Marinelli G., 1976. Geology and geothermics of the island of Milos (Greece). Technical Report. IGME, 1-58.

Fytikas, M., Innocenti, F., Kolios, N., Manetti, P., Mazzuoli, R., Poli, G., Rita, F.,Villari, L., 1986. Volcanology and petrology of volcanic products from the island of Milos and neighbouring islets. J. Volcanol. Geotherm. Res. 28, 297-317.

Gilhooly, W. P., Fike, D. A., Druschel, G. K., Kafantaris, F. C. A., Price, R. E., Amend, J. P., 2014. Sulfur and oxygen isotope insights into sulfur cycling in shallow-sea hydrothermal vents, Milos, Greece. Geochem. Trans. 15, 1-19. https://doi.org/10.1186/s12932-014-0012-y.

Godelitsas, A., Price, R.E., Pichler, T., Amend, J., Gamaletsos, P., and Göttlicher, J., 2015. Amorphous As-sulfide precipitates from the shallow-water hydrothermal vents off Milos Island (Greece). Mar. Chem. 177, 687-696, https://doi.org/10.1016/j.marchem.2015.09.004.

Godet, L., Fournier, J., Toupoint, N., and Olivier, F., 2009, Mapping and monitoring intertidal benthic habitats: a review of techniques and a proposal for a new visual methodology for the European coasts. Prog. Phys. Geog., 33, 378–402, https://doi: 10.1177/0309133309342650.

Han, C., Ye, Y., Pan Y., Qin, H., Wu, G., Chen-Tung, A. C., 2014, Spatial distribution pattern of seafloor hydrothermal vents to the southeastern Kueishan Tao offshore Taiwan Island. Acta Oceanol. Sin., 33, 37–44.

Hennenberg, M., Saghir, M.Z., Rednikov, A. Legros, J.C., 1997. Porous media and the Benard–Marangoni problem. Transport in porous media, 27, 327-355.

Houghton, J. L., Gilhooly, W. P., Kafantaris, F. C. A., Druschel, G. K., Lu, G. S., Amend, J. P., Fike, D. A., 2019. Spatially and temporally variable sulfur cycling in shallow-sea hydrothermal vents, Milos, Greece. Mar. Chem. 208, 83–94. https://doi.org/10.1016/j.marchem.2018.11.002.

Horton, C. W. Rogers, F. T., 1945. Convection currents in a porous medium. J. Appl. Phys. 16, 367–370.

Ieronimidi, E., Mertikasa, S.P., Hristopoulosa D., 2006. Fusion of Quickbird satellite images for vegetation monitoring in previously mined reclaimed areas. Conf. Paper in Proceedings of SPIE. Int. Soc. Opt. Eng. https://doi: 10.1117/12.683905.

Kiyokawa, S., Ninomiya, T., Nagata, T., Oguri, K., Ito, T., Ikehara, M., Yamaguchi, K.E., 2012. Effects of tides and weather on sedimentation of iron-oxyhydroxides in a shallow-marine hydrothermal environment at Nagahama Bay, Satsuma Iwo-Jima Island, Kagoshima, southwest Japan. Isl. Arc 21, 66–78. https://doi: 10.1111/j.1440-1738.2012.00808.x.

Kleint, C., Pichler, T., and Koschinsky, A., 2017. Geochemical characteristics, speciation and size-fractionation of iron (Fe) in two marine shallow-water hydrothermal systems, Dominica, Lesser Antilles: Chem. Geol. 454, 44–53. https://doi: 10.1016/j.chemgeo.2017.02.021.

Koedsin, W., Intararuang, W., Ritchie, R. J., Huete, A., 2016. An integrated field and remote sensing method for mapping seagrass species, cover, and biomass in Southern Thailand. Remote Sens. 8. 292. https://doi.org/10.3390/rs8040292.

Lai, K.-Y., Chen, Y.-G., Wu, Y.-M., Avouac, J.-P., Kuo, Y.-T.,Wang, Y., Chang, C.-H., Lin, K.-C., 2009. The 2005 Ilan earthquake doublet and seismic crisis in northeastern Taiwan: evidence for dyke intrusion associated with on-land propagation of the Okinawa Trough. Geophys. J. Int. 179, 678-686.

Lapwood, E.R., 1948. October. Convection of a fluid in a porous medium. In Mathematical Proceedings of the Cambridge Philosophical Society 44, 508-521. Cambridge University Press.

Lebrato, M., Wang, Y.V., Tseng, L., Achterberg, E. P., Chen, X.-G., Molinero, J.-C., Bremer, K., Westernströer, U., Söding, E., Dahms, H.-U., Küter, M., Heinath, V., Jöhnck, J., Konstantinou, K. I., Yang, Y. J., Hwang, J.-S., Garbe-Schönberg, D., 2019. Earthquake and typhoon trigger unprecedented transient shifts in shallow hydrothermal vents biogeochemistry. Sci. Rep. **9,** 16926, doi:10.1038/s41598-019-53314-y.

Liakopoulos A., 1987. Hydrothermalisme et minéralisations métallifères de l'île de Milos (Cyclades, Grèce). Université Paris-6. PhD thesis pp. 277.

Lin, C.-H., Lai, Y.-C., Shia, M.-H., Pu, H.-C., Lee, S.-J., 2018. Seismic Detection of a Magma Reservoir beneath Turtle Island of Taiwan by S-Wave Shadows and Reflections. Scientific Reports 8, 16401.

Lin, Y.-S., Lui, H. -K., Lee, J., Chen, Ch.-T. A., Burr, G. S., Chou, W.-Ch., Kuo, F.-W., 2019. Fates of vent CO_2 and its impact on carbonate chemistry in the shallow- water hydrothermal field offshore Kueishantao Islet, NE Taiwan. Mar. Chem. 210, 1-12.

Marcon, Y., Sahling, H., Allais, A.-G., Bohrmann, G., and Olu, K., 2014. Distribution and temporal variation of mega-fauna at the Regab pockmark (Northern Congo Fan), based on a comparison of videomosaics and geographic information systems analyses. Mar. Ecol. 35, 77–95, https://doi: 10.1111/maec.12056.

Mittelstaedt, E., Escartín, J., Gracias, N., Olive, J.-A., Barreyre, T., Davaille, A., Cannat, M., Garcia, R., 2012. Quantifying diffuse and discrete venting at the Tour Eiffel vent site, Lucky Strike hydrothermal field. Geochem. Geophys. Geosyst. 13, 4. https://doi: 10.1029/2011GC003991.

Naden J, Kilias, S.P., Darbyshire, D.P.F., 2005. Active geothermal systems with entrained seawater as analogues for low-sulphidation epithermal mineralization. Geology 33, 541–544. https://doi.org/10.1130/G21307.1.

Nield, D.A., Bejan, A., 2006. Convection in porous media. Vol. 3. New York: springer, pp. 640.

Nikolakopoulos, K. G., Skianis G. A., Vaiopoulos, D. A., 2007. EO-1 Hyperion and ALI bands simulation to Landsat 7 ETM+ bands and comparison, Proc. SPIE 6742, Remote sens. agric. ecosyst. hydrol. IX, 67420K. https://doi.org/10.1117/12.737941.

Nikolakopoulos, K. G., Tsombos, P. I., Skianis, G. A., Vaiopoulos D. A., 2008. EO-1 Hyperion and ALI bands simulation to Landat 7 ETM+ bands for mineral mapping in Milos Island, Proc. SPIE 7110, Remote Sensing for Environmental Monitoring, GIS Applications, and Geology VIII, 711010. https://doi.org/10.1117/12.798745.

Nomikou, P., Papanikolaou, D., Alexandri, M., Sakellariou, D., Rousakis, G., 2013. Submarine volcanoes along the aegean volcanic arc. Tectonophysics 597-598, 123-146. https://doi.org/10.1016/j.tecto.2012.10.001.

Nooner, S. L., & Chadwick, W. W., 2016. Inflation-predictable behavior and co-eruption deformation at Axial Seamount. Science 354, 1399-1403.

Osinski, G. R., Tornabene, L. L., Banerjee, N. R., Cockell, C. S., Flemming, R., Izawa, M. R. M., Southam, G., 2013. Impact-generated hydrothermal systems on Earth and Mars. Icarus 224, 347-363. https://doi.org/10.1016/j.icarus.2012.08.030.

Papanikolaou D., Lekkas E., Syskakis, D. Adamopolou E., 1993. Correlation on neotectonic structures with the geodynamic activity on Milos during the earthquakes of March 1992. Bulletin of the Geological Society of Greece 28, 413-428.

Price, R. E., Giovannelli, D., 2017. A review of the geochemistry and microbiology of marine shallow-water hydrothermal vents. Reference Module in Earth Systems and Environmental Sciences. https://doi.org/10.1016/b978-0-12-409548-9.09523-3.

Price, R.E., Savov, I., Planer-Friedrich, B., Bühring, S.I., Amend, J., Pichler, T., 2013. Processes influencing extreme as enrichment in shallow-sea hydrothermal fluids of milos island, greece: Chem. Geol. 348, 15-26. https://doi.org/10.1016/j.chemgeo.2012.06.007.

Reshitnyk, L., Costa, M., Robinson, C., Dearden, P., 2014. Evaluation of WorldView-2 and acoustic remote sensing for mapping benthic habitats in temperate coastal Pacific waters. Remote Sens. Environ. 153, 7-23. https://doi.org/10.1016/j.rse.2014.07.016.

Schipek, M., and Merkel, B.J., 2011, Continuous Monitoring of Dissolved CO2 and H2S: Technical Application in the Submarine Hydrothermal System of Panarea, Italy. Procedia Earth Planet. Sci. 4, 74–79. https://doi: 10.1016/j.proeps.2011.11.008.

Shattuck, M., Behringer, R. P., Johnson G. A., Georgiadis, J. G., 1997. Convection and flow in porous media. Part 1. Visualization by magnetic resonance imaging. J. Fluid Mech. 332, 215–245.

Skoog, A., Vlahos, P., Rogers, K. L., Amend, J. P., 2007. Concentrations, distributions, and energy yields of dissolved neutral aldoses in a shallow hydrothermal vent system of Vulcano, Italy. Org. Geochem. 38, 1416–1430. https://doi.org/10.1016/j.orggeochem.2007.03.005.

Sohn, R.A., 2007. Stochastic analysis of exit fluid temperature records from the active TAG hydrothermal mound (Mid-Atlantic Ridge, 26°N): 1. Modes of variability and implications for subsurface flow. J. Geophys. Res. 112, B07101. https://doi:10.1029/2006JB004435.

Speer, K.G., Rona, P.A., 1989. A model of an Atlantic and Pacific hydrothermal plume. J. Geophys. Res. 94, C5, 6213–6220.

Stewart, A. L., McPhie, J., 2006. Facies architecture and Late Pliocene - Pleistocene evolution of a felsic volcanic island, Milos, Greece. Bull. Volcanol. 68, 703-726. https://doi.org/10.1007/s00445-005-0045-2.

Tasaka, Y., Kudoh, Y., Takeda, Y., Yanagisawa, T., 2005. Experimental investigation of natural convection induced by internal heat generation. J. Phys. Conference Series 14, 1, IOP Publishing. pp. 168.

Tarasov, V. G., Gebruk, A.V., Mironov, A.N., Moskalev, L.I., 2005. Deep-sea and shallow-water hydrothermal vent communities: Two different phenomena? Chem. Geol. 224, 5-39. https://doi: 10.1016/j.chemgeo.2005.07.021.

Tassi, F., Capaccioni, B., Vaselli, O., 2014. Compositional spatial zonation and 2005–2013 temporal evolution of the hydrothermal-magmatic fluids from the submarine fumarolic field at Panarea Island (Aeolian Archipelago, southern Italy): J. Volcanol. Geotherm. Res. 277, 41–50. https://doi: 10.1016/j.jvolgeores.2014.03.010.

Teague, J., Miles, J., Connor, D., Priest, E., Scott, T. B., Naden, J., Nomikou, P., 2017. Exploring offshore hydrothermal venting using low-cost ROV and photogrammetric techniques: a case study from Milos Island, Greece. Preprints. https://doi.org/10.20944/preprints201710.0014.v1.

Torres-Vera, M. A., Prol-Ledesma, R. M., Canet, C., 2010. Identification of submarine hydrothermal activity using multispectral satellite images. Proc. World Geothermal Congress (Bali, Indonesia), 3 p.

Vance, S., Harnmeijer, J., Kimura, J., Hussmann H., Demartin, B., Brown, J.M., 2007. Hydrothermal systems in small ocean planets. Astrobiology 7, 987-1005. https://doi: 10.1089/ast.2007.0075.

Valsami-Jones, E., Baltatzis, E., Bailey, E. H., Boyce, A. J., Alexander, J. L., Magganas, A., Ragnarsdottir, K. V., 2005. The geochemistry of fluids from an active shallow submarine hydrothermal system: Milos island, Hellenic Volcanic Arc. J. Volcanol. Geotherm. Res. 148, 130-151. https://doi.org/10.1016/j.jvolgeores.2005.03.018.

Wenzhofer, F., Holby, O., Glud, R.N., Nielsen, H.K., and Gundersen, J.K., 2000. In situ microsensor studies of a shallow water hydrothermal vent at Milos, Greece. Mar. Chem. 69, p. 43–54.

Wilcock, W. S., Tolstoy, M., Waldhauser, F., Garcia, C., Tan, Y. J., Bohnenstiehl, D. R.,Caplan-Auerbach J., Dziak, R.P., Arnulf, A.F., Mann, M. E., 2016. Seismic constraints on caldera dynamics from the 2015 Axial Seamount eruption. Science 354, 1395-1399.

Wu, S. -F., You, C. -F., Wang, B. S., Valsami-Jones, E., Baltatzis, E. 2011. Two-cells phase separation in shallow submarine hydrothermal system at Milos Island, Greece: Boron isotopic evidence. Geophys. Res. Lett. 38, 3-7. https://doi.org/10.1029/2011GL047409.

Wu, S.-F., You, C.-F., Yen-Po, L., Valsami-Jones, E., Baltatzis, E., 2016. New boron isotopic evidence for sedimentary and magmatic fluid influence in the shallow hydrothermal vent system of Milos Island (Aegean Sea, Greece). J. Volcanol. Geotherm. Res. 310, 58-71. https://doi.org/10.1016/j.jvolgeores.2015.11.013.

Yang, L., Hong, H., Guo, W., Chen, C. T. A., Pan, P. I., Feng, C. C., 2012. Absorption and fluorescence of dissolved organic matter in submarine hydrothermal vents off NE Taiwan. Mar. Chem. 128-129, 64-71. https://doi.org/10.1016/j.marchem.2011.10.003.

Yücel M., Sievert S.M., Vetriani C., Foustoukos D.I., Giovannelli D., Le Bris N., 2013. Eco-geochemical dynamics of a shallow-water hydrothermal vent system at Milos Island, Aegean Sea (Eastern Mediterranean). Chem. Geol. 356, 11-20.

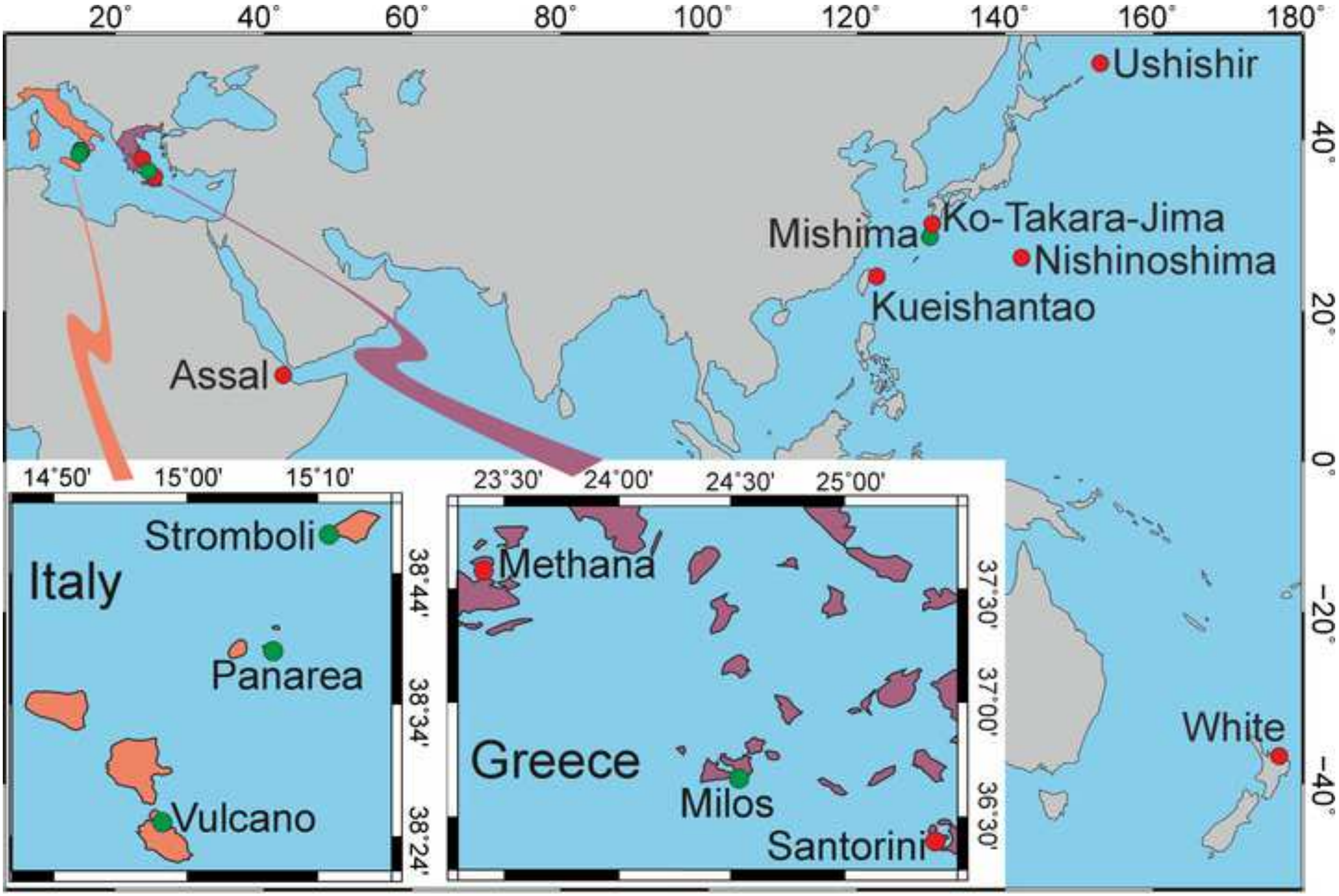
20°
40°
60°
80°
100°
120°
140°
160°
180°
40°
20°
0°
-20°
-40°
Ushishir
Ko-Takara-Jima
Mishima
Nishinoshima
Kueishantao
Assal
White
14°50'
15°00'
15°10'
38°44'
38°34'
38°24'
Italy
Stromboli
Panarea
Vulcano
23°30'
24°00'
24°30'
25°00'
37°30'
37°00'
36°30'
Greece
Methana
Milos
Santorini

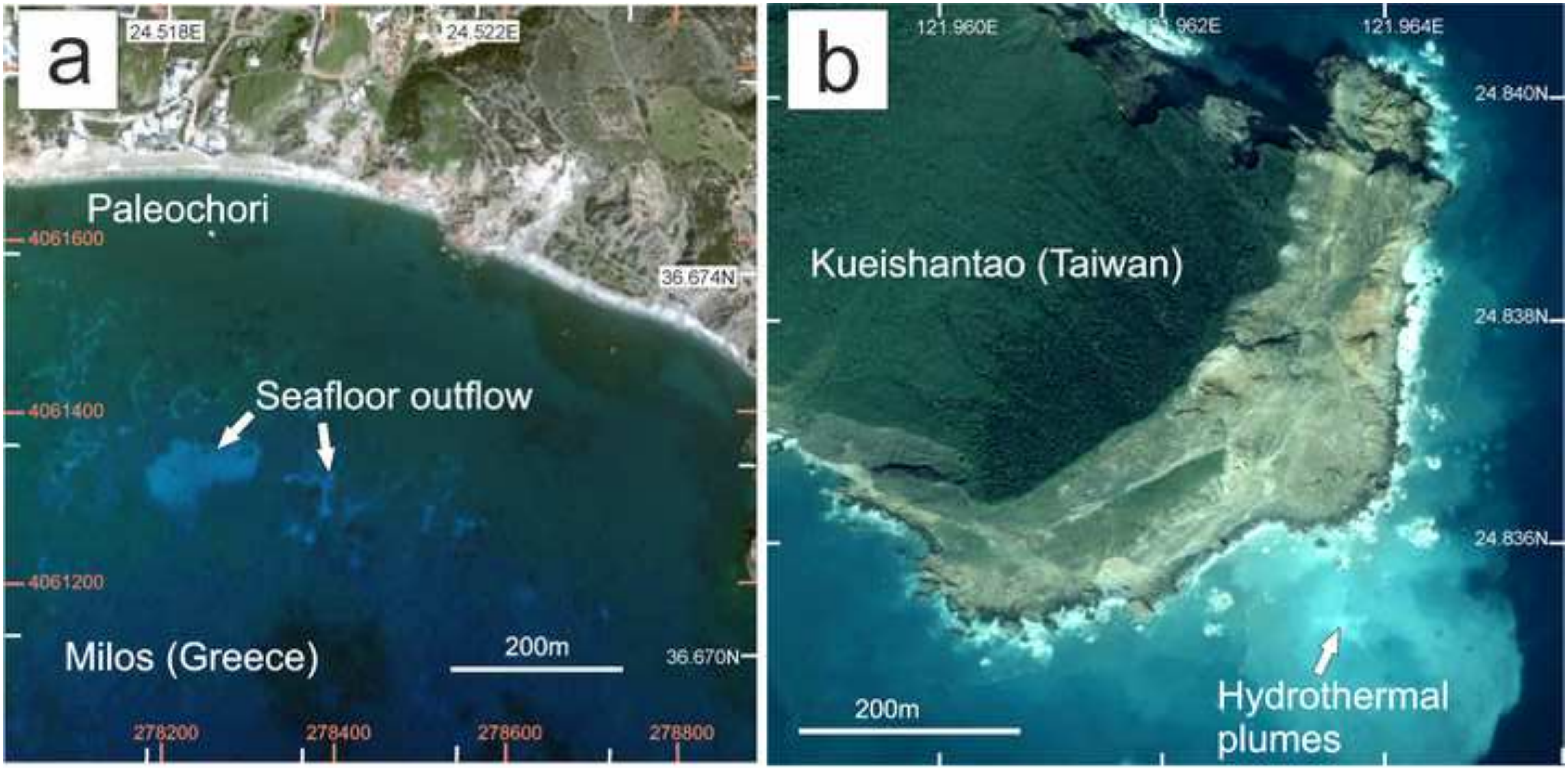
a
24.518E
24.522E
Paleochori
4061600
36.674N
Seafloor outflow
4061400
4061200
Milos (Greece)
200m
36.670N
278200
278400
278600
278800
b
121.960E
121.962E
121.964E
24.840N
Kueishantao (Taiwan)
24.838N
24.836N
200m
Hydrothermal
plumes

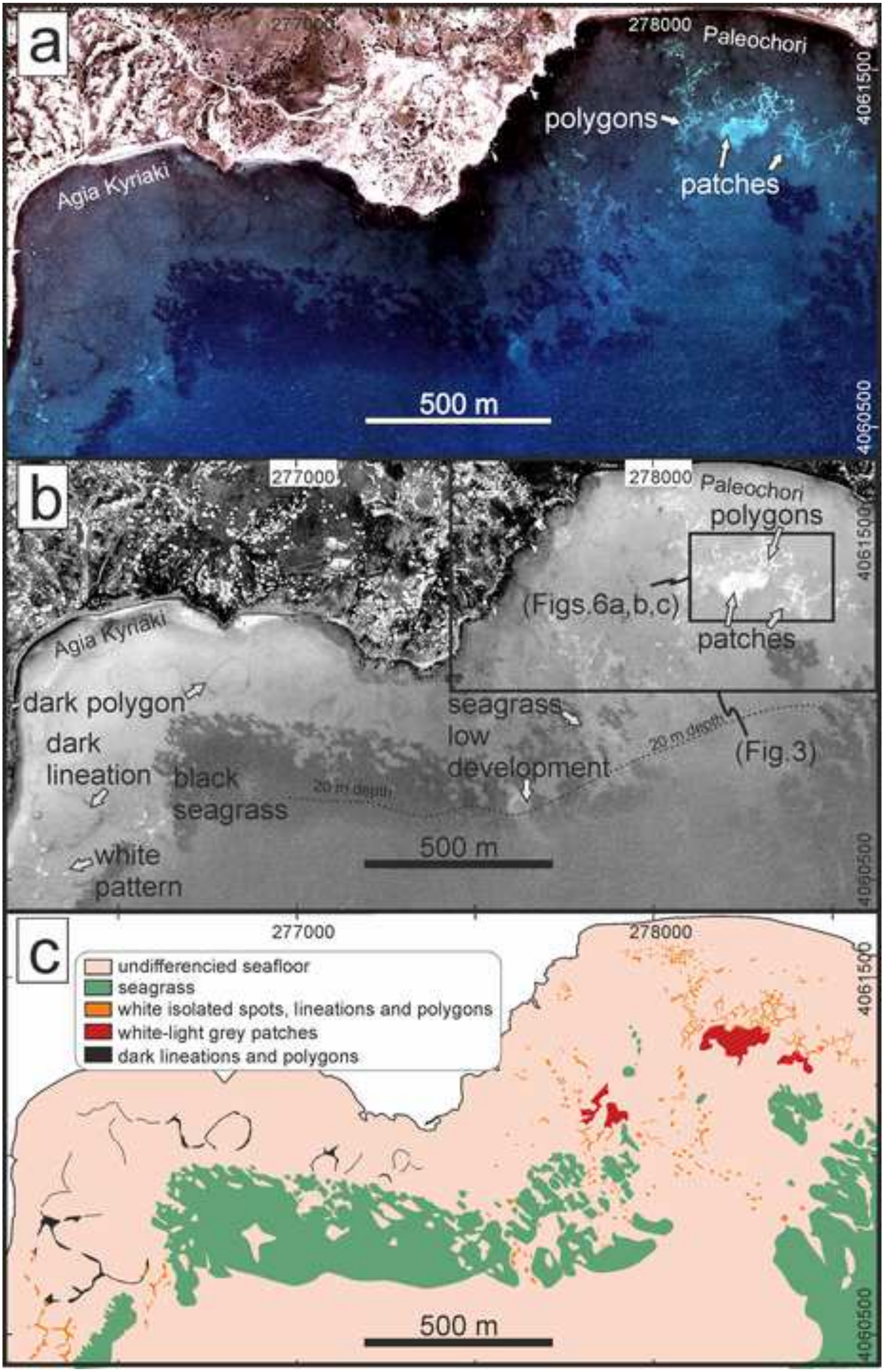
a
277000
278000
Paleochori
4061500
polygons
patches
Agia Kyriaki
500 m
4060500
b
277000
278000
Paleochori
polygons
4061500
(Figs.6a,b,c)
patches
Agia Kyriaki
dark polygon
seagrass
low
development
20 m depth
(Fig.3)
dark
lineation
black
seagrass
20 m depth
500 m
white
pattern
4060500
c
277000
278000
undifferencied seafloor
seagrass
white isolated spots, lineations and polygons
white-light grey patches
dark lineations and polygons
4061500
500 m
4060500

Figure 5 tiff

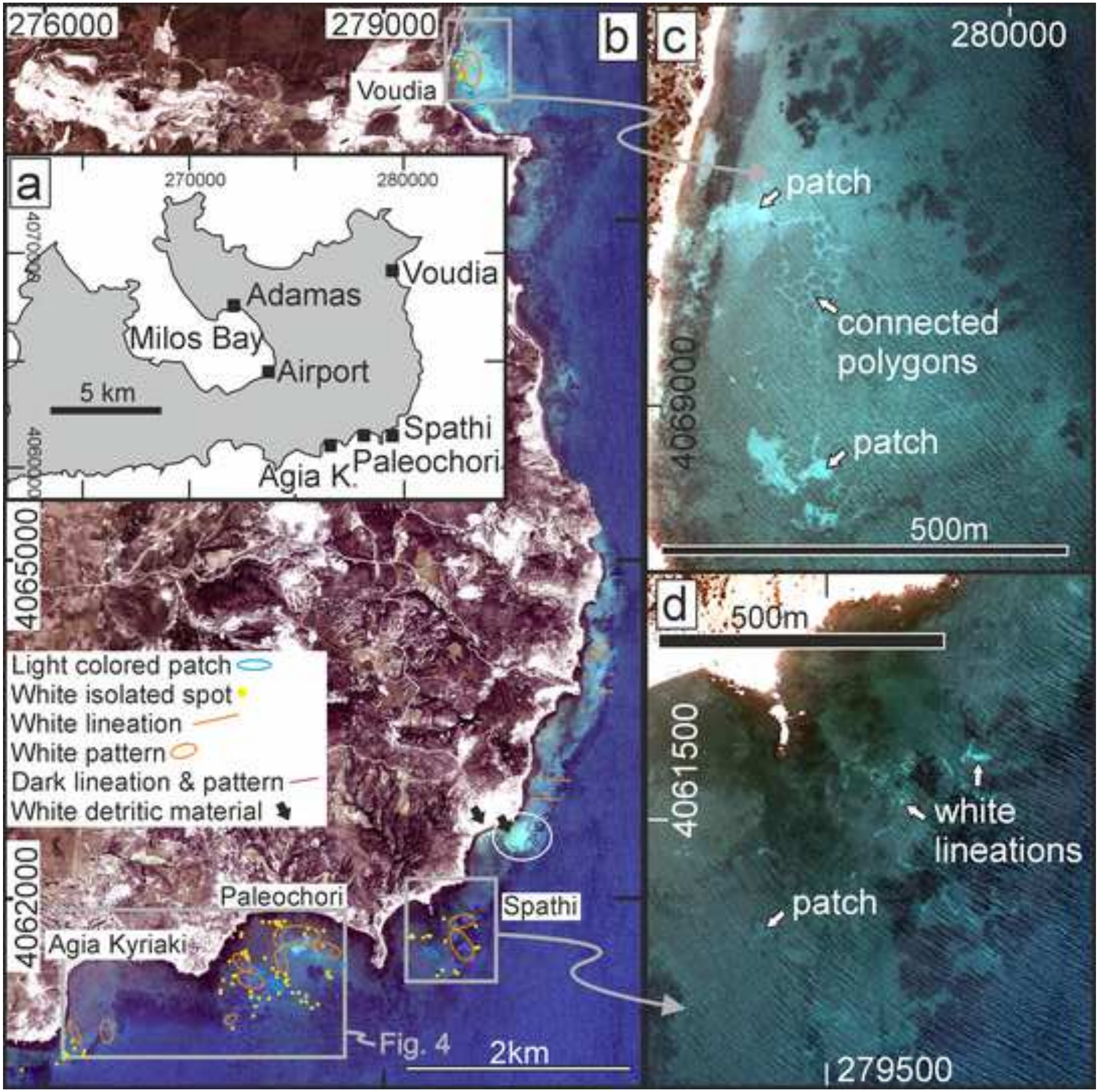

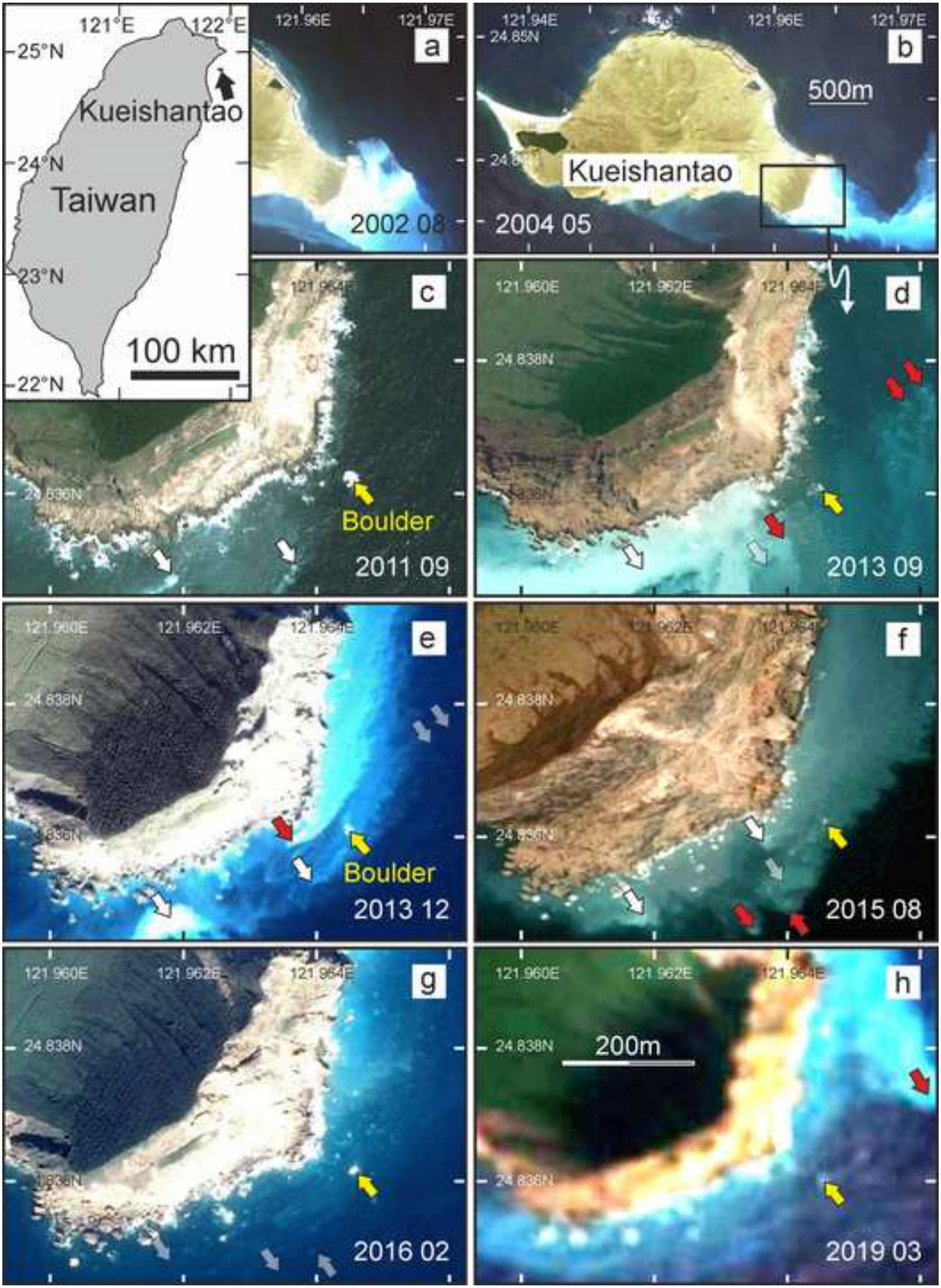
121°E
122°E
25°N
24°N
23°N
22°N
Kueishantao
Taiwan
100 km
121.96E
121.97E
a
2002 08
121.94E
24.85N
121.96E
121.97E
b
500m
24.84N
Kueishantao
2004 05
121.964E
c
24.836N
Boulder
2011 09
121.960E
121.962E
121.964E
d
24.838N
24.836N
2013 09
121.960E
121.962E
121.964E
e
24.838N
24.836N
Boulder
2013 12
121.960E
121.962E
121.964E
f
24.838N
24.836N
2015 08
121.960E
121.962E
121.964E
g
24.838N
24.836N
2016 02
121.960E
121.962E
121.964E
h
24.838N
200m
24.836N
2019 03

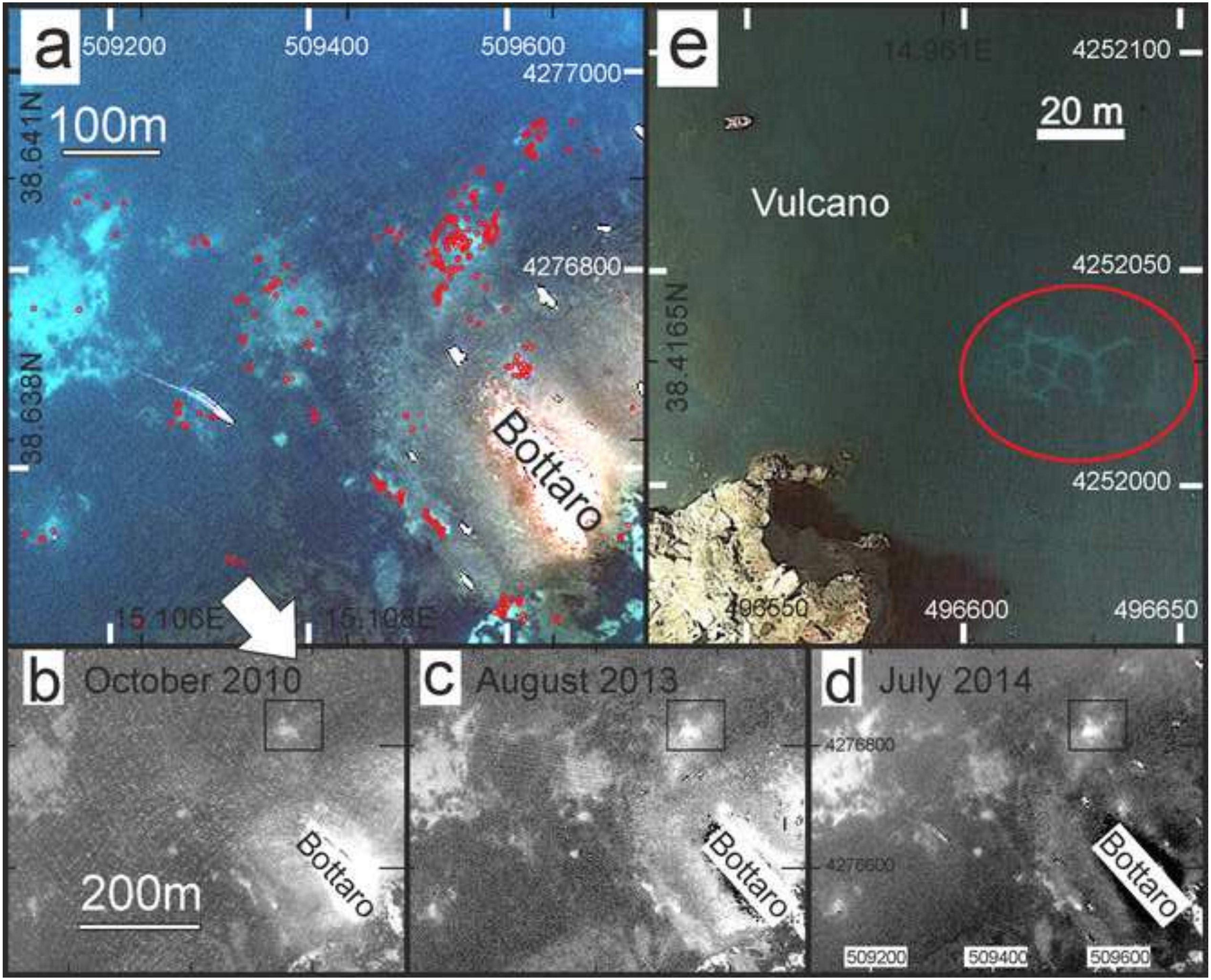
a
509200
509400
509600
4277000
100m
38.641N
4276800
38.638N
Bottaro
15.106E
15.108E
e
14.961E
4252100
20 m
Vulcano
4252050
38.4165N
4252000
496550
496600
496650
b
October 2010
200m
Bottaro
c
August 2013
Bottaro
d
July 2014
4276800
4276600
Bottaro
509200
509400
509600